Probing Maxwell's Demon with a Nanoscale Thermometer

Justin P. Bergfield,[†,*] Shauna M. Story,[‡] Robert C. Stafford,[‡] and Charles A. Stafford[‡]

[†]Department of Chemistry, Northwestern University, 1818 Hinman Avenue, Evanston, Illinois 60208, United States and [‡]Department of Physics, University of Arizona, 1118 East Fourth Street, Tucson, Arizona 85721, United States

ABSTRACT A precise definition for a quantum electron thermometer is given, as an electron reservoir coupled locally (*e.g.*, by tunneling) to a sample, and brought into electrical and thermal equilibrium with it. A realistic model of a scanning thermal microscope with atomic resolution is then developed, including the effect of thermal coupling of the probe to the ambient environment. We show that the temperatures of individual atomic orbitals or bonds in a conjugated molecule with a temperature gradient across it exhibit quantum oscillations, whose origin can be traced to a realization of Maxwell's demon at the single-molecule level. These oscillations may be understood in terms of the rules of covalence describing bonding in π-electron systems. Fourier's law of heat conduction is recovered as the resolution of the temperature probe is reduced, indicating that the macroscopic law emerges as a consequence of coarse graining.

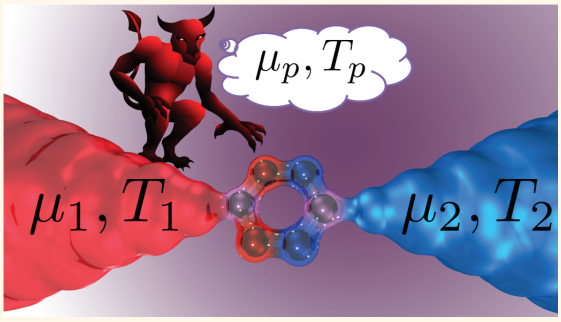

KEYWORDS: quantum thermometer · scanning thermal microscope (SThM) · three-terminal heat transport theory · definition of temperature · single-molecule heat transport · thermoelectric effects · Fourier's law · rules of covalence

Recent advances in thermal microscopy[1−5] have opened the door to understanding nonequilibrium thermodynamics at the nanoscale. The nonequilibrium temperature distribution in a quantum system subject to a thermal or electric gradient can now be probed experimentally, raising a number of fundamental questions: Can significant temperature variations occur across individual atoms or molecules without violating the uncertainty principle? How are the electronic and lattice temperatures related in a nanostructure out of thermal equilibrium? How does the classical Fourier law of heat conduction emerge[6,7] from this quantum behavior in the macroscopic limit?

In order to address these questions theoretically, a definition of a nanoscale thermometer that is both realistic and mathematically rigorous is needed. According to the principles of thermodynamics, a thermometer is a small system (probe) with some readily identifiable temperature-dependent property that can be brought into thermal equilibrium with the system of interest (sample). Once thermal equilibrium is established, the net heat current between probe and sample vanishes,[8−10] and the resulting temperature of the probe constitutes a *measurement of the sample temperature*. High spatial and thermal resolution require that the thermal coupling between probe and sample is local[4] and that the coupling between the probe and the ambient environment is small,[2] respectively.

It should be emphasized that, out of equilibrium, the temperature distributions of different microscopic degrees of freedom (*e.g.*, electrons and phonons) do not, in general, coincide, so that one has to distinguish between measurements of the electron temperature[8,11] and the lattice temperature.[10,12] This distinction is particularly acute in the extreme limit of elastic quantum transport,[13] where electron and phonon temperatures are completely decoupled.

In this article, we develop a realistic model of a scanning thermal microscope (SThM) operating in the tunneling regime in ultrahigh vacuum, where the vacuum tunneling gap ensures that phonon heat conduction to the probe is negligible. Since electrons carry both charge and heat, an additional condition is necessary to define an electron thermometer. We proceed by noting that, as a practical matter, in order to reduce the thermal coupling of the thermometer to the

* Address correspondence to justin.bergfield@northwestern.edu.

Received for review February 28, 2013 and accepted April 21, 2013.

Published online May 07, 2013
10.1021/nn401027u

ambient environment, it should form an open electrical circuit (or have very high impedance to ground). This ensures that, in addition to the heat current, the electrical current between sample and probe vanishes. This second condition is also necessary to ensure the thermometer is in local equilibrium with the sample. An electron thermometer is thus defined as an electron reservoir whose temperature is fixed by the conditions of electric and thermal equilibrium with the sample:

$$I_p^{(\nu)} = 0,\ \nu = 0, 1 \qquad (1)$$

where $I_p \equiv -eI_p^{(0)}$ and $I_p^Q \equiv I_p^{(1)}$ are the electric current and heat current, respectively, flowing into the probe. In an ideal measurement, the sample would be the sole source of charge and heat flowing into the probe, but we also consider nonideal measurements, where there is an additional thermal coupling to the ambient environment. In practice, this coupling plays a crucial role in limiting the resolution of temperature measurements.[4]

In a measurement of the temperature distribution in a conductor subject to thermal and/or electric gradients, the electron thermometer thus serves as an open third terminal in a three-terminal thermoelectric circuit, a generalization of Büttiker's voltage probe concept[14] (see Figure 1). Note that the conditions of eq 1 allow a local temperature to be defined under general thermoelectric bias conditions, relevant for the analysis of nonequilibrium thermoelectric device performance.[15−18]

Previous theoretical analyses of quantum electron thermometers either completely neglected thermoelectric effects[8,9,19] or considered the measurement scenario of eq 1 as only one of several possible cases,[20−23] without giving definitive arguments for one case over the others. The subtle definition of local temperature given in ref 11 (thermometer causes minimal perturbation of system dynamics), on the other hand, may capture the spirit of our two separate conditions, at some level. A recent review of the topic is given in ref 24. To our knowledge, a theoretical analysis of the effect of finite coupling of the temperature probe to the ambient environment has not previously been undertaken.

Using our model of a nanoscale electron thermometer, we investigate the nonequilibrium temperature distributions in single-molecule junctions subject to a thermal gradient. Quantum temperature oscillations analogous to those predicted in one-dimensional systems[11] are predicted in molecular junctions for several different conjugated organic molecules and are explained in terms of the rules of covalence describing bonding in π-conjugated systems. In terms of directing the flow of heat, the rules of covalence can be seen as an embodiment of Maxwell's demon at the single-molecule level.

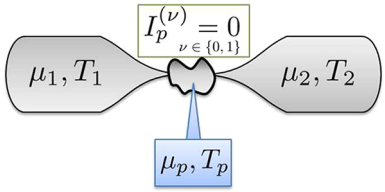

Figure 1. Schematic representation of a temperature probe as an open third terminal of a thermoelectric circuit.

It has been argued that in some systems quantum temperature oscillations can be washed out by either dephasing[6] or disorder,[7] leading to restoration of Fourier's classical law of heat conduction. However, in molecular junctions the required scattering would be so strong as to dissociate the molecule. We investigate the effect of finite spatial resolution on the nonequilibrium temperature distribution and find that Fourier's law emerges naturally as a consequence of coarse-graining of the measured temperature distribution. Thus our resolution of the apparent contradiction between Fourier's macroscopic law of heat conduction and the predicted nonmonotonic temperature variations at the nanoscale is that the quantum temperature oscillations are really there, provided the temperature measurement is carried out with sufficient resolution to observe them, but that Fourier's law emerges naturally when the resolution of the thermometer is reduced.

This paper is organized as follows: We first derive a general linear-response formula for an electron thermometer. A realistic model of a scanning thermal microscope with sub-nanometer resolution is then developed, including a discussion of thermal coupling of the probe to the environment. Finally, results for the nonequilibrium temperature distributions in several single-molecule junctions subject to a thermal gradient are presented, and the implications of our findings are discussed.

RESULTS AND DISCUSSION

Electronic Temperature Probe. Consider a general system with M electrical contacts. Each contact α is connected to a reservoir at temperature T_α and electrochemical potential μ_α. In linear response, the electrical current $-eI_\alpha^{(0)}$ and heat current $I_\alpha^{(1)}$ flowing into reservoir α may be expressed as

$$I_\alpha^{(\nu)} = \sum_{\beta=1}^{M} \left[\mathscr{L}_{\alpha\beta}^{(\nu)}(\mu_\beta - \mu_\alpha) + \frac{\mathscr{L}_{\alpha\beta}^{(\nu+1)}}{T}(T_\beta - T_\alpha) \right] \qquad (2)$$

where $\mathscr{L}_{\alpha\beta}^{(\nu)}$ is an Onsager linear-response coefficient. Equation 2 is a *completely general* linear-response formula and applies to macroscopic systems, mesoscopic systems, nanostructures, *etc.*, including electrons, phonons, and all other degrees of freedom, with arbitrary interactions between them. For a discussion of this general linear-response formula applied to bulk systems, see ref 25.

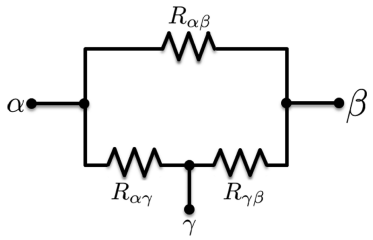

Figure 2. Equivalent circuit for $\tilde{\mathscr{T}}^{(0)}_{\alpha\beta}$ and $\mathscr{T}^{(0)}$, where the resistance $R_{\alpha\beta} = [e^2\mathscr{T}^{(0)}_{\alpha\beta}]^{-1}$. $e^2\mathscr{T}^{(0)}$ is the loop conductance of the circuit and $e^2\tilde{\mathscr{T}}^{(0)}_{\alpha\beta}$ is the effective two-terminal conductance between terminals α and β.

In this article, we consider systems driven out of equilibrium by a temperature gradient between reservoirs 1 and 2. Thermoelectric effects are included, so the chemical potentials of the various reservoirs may differ. We consider pure thermal circuits (*i.e.*, open electrical circuits), for which $I^{(0)}_\alpha = 0\ \forall\ \alpha$. These conditions may be used to eliminate the chemical potentials μ_α from eq 2, leading to a simpler formula for the heat currents:

$$I^Q_\alpha \equiv I^{(1)}_\alpha = \sum_{\beta=1}^{3} \tilde{\kappa}_{\alpha\beta}(T_\beta - T_\alpha) \tag{3}$$

In the absence of an external magnetic field $\mathscr{T}^{(\nu)}_{\alpha\beta} = \mathscr{T}^{(\nu)}_{\beta\alpha}$ and the three-terminal thermal conductances are given by

$$\tilde{\kappa}_{\alpha\beta} = \frac{1}{T}\left[\mathscr{T}^{(2)}_{\alpha\beta} - \frac{[\mathscr{T}^{(1)}_{\alpha\beta}]^2}{\tilde{\mathscr{T}}^{(0)}_{\alpha\beta}} - \mathscr{T}^{(0)}\left(\frac{\mathscr{T}^{(1)}_{\alpha\gamma}\mathscr{T}^{(1)}_{\alpha\beta}}{\mathscr{T}^{(0)}_{\alpha\gamma}\mathscr{T}^{(0)}_{\alpha\beta}} + \frac{\mathscr{T}^{(1)}_{\gamma\beta}\mathscr{T}^{(1)}_{\alpha\beta}}{\mathscr{T}^{(0)}_{\gamma\beta}\mathscr{T}^{(0)}_{\alpha\beta}} - \frac{\mathscr{T}^{(1)}_{\alpha\gamma}\mathscr{T}^{(1)}_{\gamma\beta}}{\mathscr{T}^{(0)}_{\alpha\gamma}\mathscr{T}^{(0)}_{\gamma\beta}}\right)\right] \tag{4}$$

with

$$\tilde{\mathscr{T}}^{(0)}_{\alpha\beta} = \mathscr{T}^{(0)}_{\alpha\beta} + \frac{\mathscr{T}^{(0)}_{\alpha\gamma}\mathscr{T}^{(0)}_{\gamma\beta}}{\mathscr{T}^{(0)}_{\alpha\gamma} + \mathscr{T}^{(0)}_{\gamma\beta}} \tag{5}$$

and

$$\frac{1}{\mathscr{T}^{(0)}} = \frac{1}{\mathscr{T}^{(0)}_{12}} + \frac{1}{\mathscr{T}^{(0)}_{13}} + \frac{1}{\mathscr{T}^{(0)}_{23}} \tag{6}$$

An equivalent circuit for $\tilde{\mathscr{T}}^{(0)}_{\alpha\beta}$ and $\mathscr{T}^{(0)}$ is given in Figure 2.

The first line of eq 4 resembles the familiar two-terminal thermal conductance[17,26,27] $\kappa_{\alpha\beta} = [\mathscr{T}^{(2)}_{\alpha\beta} - (\mathscr{T}^{(1)}_{\alpha\beta})^2/\mathscr{T}^{(0)}_{\alpha\beta}]/T$ with $\mathscr{T}^{(0)}_{\alpha\beta}$ replaced by eq 5. Since $\mathscr{T}^{(2)}_{\alpha\beta}$ is usually the dominant term, $\tilde{\kappa}_{\alpha\beta}$ is often comparable to the two-terminal form $\kappa_{\alpha\beta}$ (*cf.* Figure 6). However, the discrepancy is sizable in some cases. Although it might be tempting to interpret the second line in eq 4 as a nonlocal quantum correction to the thermal conductance, it should be emphasized that this is a generic three-terminal thermoelectric effect that arises in bulk systems as well as nanostructures.

Temperature Measurement. In addition to the coupling of the temperature probe to the system of interest, we assume the probe also has a small thermal coupling κ_{p0} to the environment at temperature T_0. The environment could be, for example, the blackbody radiation or gaseous atmosphere surrounding the circuit or the cantilever/driver on which the temperature probe is mounted. The heat current flowing from the environment into the probe must be added to eq 3 to determine the total heat current:

$$I^Q_p = \sum_{\beta=1}^{2} \tilde{\kappa}_{p\beta}(T_\beta - T_p) + \kappa_{p0}(T_0 - T_p) \tag{7}$$

Thermal coupling to the environment is important when the coupling to the system is weak, and it is a limiting factor in the thermal resolution of any temperature probe. The environment is effectively a fourth terminal in the thermoelectric circuit; however, we consider only thermal coupling of the probe to the environment, so the thermal conductances $\tilde{\kappa}_{p1}$, $\tilde{\kappa}_{p2}$ in eq 7 have the three-terminal form (eq 4). Solving eqs 1 and 7 for the temperature, we find

$$T_p = \frac{\tilde{\kappa}_{p1}T_1 + \tilde{\kappa}_{p2}T_2 + \kappa_{p0}T_0}{\tilde{\kappa}_{p1} + \tilde{\kappa}_{p2} + \kappa_{p0}} \tag{8}$$

for a probe in thermal and electrical equilibrium with, and coupled locally to, a system of interest. Experimentally, the reduction of the thermal response of the probe at finite κ_{p0} is characterized by the sensitivity:[4]

$$S \equiv \frac{\partial T_p}{\partial T_s} = \frac{\kappa_{ps}}{\kappa_{ps} + \kappa_{p0}} \tag{9}$$

where T_s is the sample temperature and $\kappa_{ps} = \tilde{\kappa}_{p1} + \tilde{\kappa}_{p2}$ is the total thermal conductance between the probe and the sample. Equation 9 follows directly from eq 8 with $T_1 = T_2 = T_s$.

Equations 4 and 8 provide a *general definition of an electron thermometer* coupled to a system with a temperature gradient across it, in the linear response regime. Equation 8 can be rewritten in the following instructive form:

$$T_p = T_0 + S(\bar{T} - T_0) + C\Delta T/2 \tag{10}$$

where $T_1 = \bar{T} + \Delta T/2$, $T_2 = \bar{T} - \Delta T/2$, S is the sensitivity, and C is the contrast defined by

$$C = \frac{\tilde{\kappa}_{p1} - \tilde{\kappa}_{p2}}{\tilde{\kappa}_{p1} + \tilde{\kappa}_{p2} + \kappa_{p0}} \tag{11}$$

For the case of a symmetric thermal bias ($\bar{T} = T_0$), $T_p - T_0$ is proportional to the contrast, and the second term on the right-hand side of eq 10 is zero. A symmetric thermal bias is of particular interest from a theoretical point of view, but may be difficult to realize in the laboratory, where it is common to heat one electrode and keep the other electrode at ambient temperature; $T_1 = T_0 + \Delta T$, $T_2 = T_0$. Here we point out that it is possible to extract the quantity of theoretical interest C (*i.e.*, quantum temperature oscillations) from a

sequence of two measurements: (a) where both electrodes are heated, $T_1 = T_2 = T_0 + \Delta T$, yielding $T_p^{(a)} = T_0 + S\Delta T$; and (b) where only one electrode is heated, $T_1 = T_0 + \Delta T, T_2 = T_0$, yielding $T_p^{(b)} = T_0 + S\Delta T/2 + C\Delta T/2$. Then $2T_p^{(b)} - T_p^{(a)} = T_0 + C\Delta T$. In the remainder of this article, we focus on the case of a symmetric thermal bias. Explicit results for a junction where one electrode is heated and the other is kept at ambient temperature are given in the Supporting Information.

Quantum Electron Thermometer. We consider nanoscale junctions with weak electron−phonon coupling operating near room temperature. Under linear-response conditions, electron−phonon interactions and inelastic scattering are weak in such systems, and the indirect phonon contributions to $\mathscr{T}_{\alpha\beta}^{(0)}$ and $\mathscr{T}_{\alpha\beta}^{(1)}$ can be neglected, while the direct phonon contribution to $\mathscr{T}_{p\beta}^{(2)}$ is negligible due to the vacuum tunneling gap. The linear response coefficients needed to evaluate eq 8 may thus be calculated using elastic electron transport theory:[17,26,27]

$$\mathscr{T}_{\alpha\beta}^{(\nu)} = \frac{1}{h}\int dE(E-\mu_0)^{\nu} T_{\alpha\beta}(E)\left(-\frac{\partial f_0}{\partial E}\right) \qquad (12)$$

where f_0 is the equilibrium Fermi−Dirac distribution of the electrodes at chemical potential μ_0 and temperature T_0. The transmission function may be expressed as[13,28]

$$T_{\alpha\beta}(E) = \mathrm{Tr}\{\Gamma^{\alpha}(E)\, G(E)\, \Gamma^{\beta}(E)\, G^{\dagger}(E)\} \qquad (13)$$

where $\Gamma^{\alpha}(E)$ is the tunneling-width matrix for lead α and $G(E)$ is the retarded Green's function of the junction.

SPM-Based Temperature Probe of a Single-Molecule Junction. As an electron thermometer with atomic-scale resolution, we propose using a scanning probe microscope (SPM) with an atomically sharp conducting tip mounted on an insulating piezo actuator designed to minimize the thermal coupling to the environment. The tip could serve, for example, as a bolometer or thermocouple,[4] and its temperature could be read out electrically using ultrafine shielded wiring. The proposed setup is essentially a nanoscale version of the commercially available SThM and is analogous to the ground-breaking SThM with 10 nm resolution developed by Kim *et al.*,[4] but operating in the tunneling regime rather than the contact regime.

Such an atomic-resolution electron thermometer could be used to probe the local temperature distribution in a variety of nanostructures/mesoscopic systems out of equilibrium. In the following, we focus on the specific example of a single-molecule junction (SMJ) subject to a temperature gradient, with no electrical current flowing. In particular, we consider junctions containing conjugated organic molecules, the relevant electronic states of which are determined by the π-orbitals. We consider transition metal tips, where

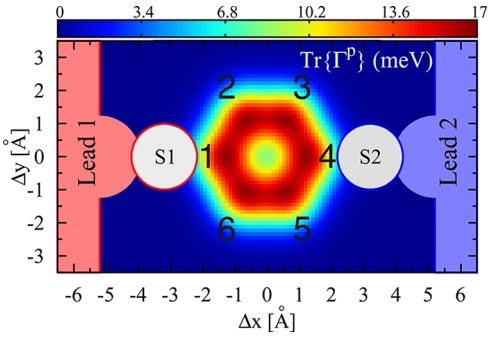

Figure 3. Calculated spatial map of $\mathrm{Tr}\{\Gamma^{p}\}$ for a Pt electron thermometer scanned 3.5 Å above the plane of a benzene molecule and a schematic representation of a *para*-benzenedithiol ([1,4]BDT) junction. Peak values of $\mathrm{Tr}\{\Gamma^{p}\} \approx 16.6$ meV correspond to the centers of the carbon atoms, which are numbered in black. The sulfur and gold atoms were drawn using their covalent radii of 102 and 134 pm, respectively.

tunneling is dominated by the d-like orbitals of the apex atom.[29]

The tunnel coupling between the tip of the electronic temperature probe and the π-system of the molecule is described by the tunneling-width matrix[29,30]

$$\Gamma_{nm}^{p}(E) = 2\pi V_n V_m^{*} \rho_p(E) \qquad (14)$$

where n and m label π-orbitals of the molecule, $\rho_p(E)$ is the local density of states on the apex atom of the probe, and V_m is the tunneling matrix element between the evanescent tip wave function and orbital m of the molecule. Since the temperature probe is in the tunneling regime, and not the contact regime, the phonon contribution to the transport vanishes; heat is exchanged between system and probe only *via* the electron tunneling characterized by Γ^{p}.

In Figure 3, the trace of $\Gamma^{p}(E_F)$ is shown for a Pt temperature probe held 3.5 Å above the plane of a Au−[1,4]benzenedithiol−Au ([1,4]BDT) molecular junction. A schematic of the [1,4]BDT junction is also shown, with sulfur and gold atoms drawn to scale using their covalent radii of 102 and 134 pm, respectively. Peaks in $\mathrm{Tr}\{\Gamma^{p}\}$ correspond to the locations of carbon π-orbitals, labeled with black numbers. Γ^{p} determines the tunneling transmission probabilities through eq 13 and the thermoelectric response coefficients through eq 12. These in turn determine the measured temperature through eqs 4 and 8.

The density of states (DOS) of the Au−para BDT−Au junction is shown in Figure 4, simulated using our many-body theory including the electrostatic influence of the thiol end groups. Our many-body theory accurately reproduces the fundamental gap of gas-phase benzene (~10.4 eV), allowing us to unambiguously determine the energy-level alignment between the electrodes and molecule. Transport occurs within the HOMO−LUMO gap, but is dominated by the

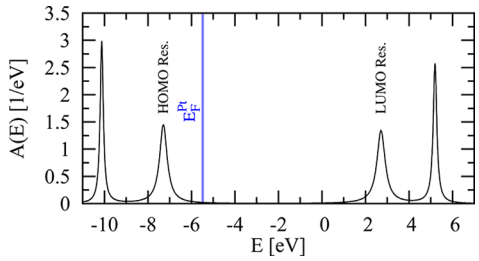

Figure 4. Spectral function $A(E) = -1/\pi$ Im Tr$\{G\}$ of a Au−[1,4]BDT−Au (para) junction in the vicinity of the HOMO and LUMO resonances, calculated using many-body theory including the effect of the partially charged sulfur atoms on the intramolecular potential. In all benzene simulations $\Gamma_1 = \Gamma_2 = 0.69$ eV and the excess charge on the thiol end-groups $\approx -0.29e$, values that give the best agreement with the measured thermopower[16] and linear-response conductance[31] measurements. The blue line indicates the Pt probe's Fermi energy, $E_F^{Pt} = -5.53$ eV, averaged over the [110], [111], [320], and [331] crystal planes.[32]

HOMO resonance. This is true for all of the molecular junctions considered in this article.

Coupling to the Environment. The thermal coupling κ_{p0} of the temperature probe to the ambient environment places stringent limits on the thermal resolution of a SThM.[2,4] An accurate temperature measurement requires either sensitivity $S \approx 1$ ($\kappa_{ps} \gg \kappa_{p0}$), so that $T_p \approx T_s$, or $S \approx$ const, so that it may be taken as a constant correction factor.[4] In the tunneling regime investigated in the present work, we shall see that $S \neq$ const, so that accurate temperature measurements require high sensitivity. Nonetheless, we demonstrate that the qualitative features of the nonequilibrium temperature distribution can be faithfully captured even when $S \ll 1$.

In the simulations presented here, we consider both a very weak environmental coupling ($\kappa_{p0} = 10^{-4}\kappa_0$, for which $S \approx 1$ over much of the sample) and a fairly strong environmental coupling ($\kappa_{p0} = 10\kappa_0$, for which $S \ll 1$). Here $\kappa_0 = (\pi^2/3)(k_B^2 T/h) = 2.84 \times 10^{-10}$ W/K is the thermal conductance quantum.[31,32] For comparison, the UHV SThM of Kim *et al.*[4] recently achieved $\kappa_{p0} \approx 700\kappa_0$. Observation of the quantum effects on the nonequilibrium temperature distribution predicted theoretically[11] and investigated in this work would require a significant reduction of κ_{p0} compared to the current experimental state of the art, not unlike the push to observe quantum effects in nanofabricated oscillators.[35]

There are both practical and fundamental limits on κ_{p0}. In a gaseous atmosphere, SThM resolution is limited by convection.[2] In the UHV SThM of ref 4, κ_{p0} is dominated by conduction through the cantilever upon which the temperature probe is mounted. A fundamental limitation is radiative coupling to the ambient blackbody environment, for which

$$\kappa_{p0} = 4\varepsilon A \sigma T_0^3 \qquad (15)$$

where ε and A are the emissivity and surface area, respectively, of the metal tip, and $\sigma = (\pi^2 k_B^4/60\hbar^3 c^2)$ is the Stefan−Boltzmann constant. The ratio

$$\frac{\kappa_{p0}}{\kappa_0} = \frac{2\pi\varepsilon A}{5}\left(\frac{k_B T_0}{\hbar c}\right)^2 \overset{T_0 = 300K}{=} \frac{2.1\varepsilon A}{(10\ \mu m)^2} \qquad (16)$$

The conducting tip of the temperature probe must thus have linear dimensions $R \lesssim 10\ \mu$m in order to resolve quantum effects at room temperature. A conducting tip of small volume will also ensure rapid equilibration of the probe with the sample (see Methods section).

We do not include the direct radiative contribution to $\tilde{\kappa}_{p1}$ and $\tilde{\kappa}_{p2}$. Since the separation between electrodes 1 and 2 is much less than the photon thermal wavelength, we consider that blackbody radiation from the two electrodes contributes to a common ambient environment at temperature $\bar{T} = T_0$. Near-field effects may lead to an increase of κ_{p0} over the value given by eq 15, but the contribution to κ_{p0} due to near-field radiation is nonetheless estimated to be quite small[1] and slowly varying spatially compared to electronic processes. We do not consider radiative coupling of the probe to the molecule itself due to the strong quantum suppression of radiative heat transfer for structures smaller than the thermal wavelength.[36]

Nonequilibrium Temperature Distributions. In this section, we investigate the spatial temperature profiles for three Au−benzenedithiol−Au (BDT) junction geometries, a linear [1,6]hexatrienedithiol junction, and a polycyclic [2,7]pyrenedithiol junction. The BDT and hexatriene SMJ calculations were performed using a molecular Dyson equation many-body transport theory[13] in which the molecular π-system is solved exactly, including all charge and excited states, and the lead-molecule tunneling is treated to infinite order (see Methods section). The transport calculations for the pyrene junction were performed using Hückel theory (see Supporting Information). In all cases, the ambient temperature is taken as $T_0 = 300$ K.

Benzenedithiol Junctions. We investigate the temperature distributions for three Au−benzenedithiol−Au (BDT) junction geometries: the "para" [1,4]BDT junction, shown schematically along with the trace of the lead-molecule coupling matrix in Figure 3, the "ortho" [1,2]BDT junction, and the "meta" [1,3]BDT junction. The calculated spatial temperature distribution for each junction configuration is shown in Figure 5, for both weak and strong environmental couplings, with $T_1 = 325$ K and $T_2 = 275$ K. The figure illustrates quantum oscillations of the local temperature near the molecules, which are clearly resolvable using our model of a nanoscale electron thermometer. In each junction, the π-orbitals of the molecule have a characteristic temperature different from that of its nearest neighbors. For instance, in the para junction orbitals 2 and 6 are hot, orbitals 3 and 5 are cold, while orbitals 1 and 4, directly connected to the hot and cold

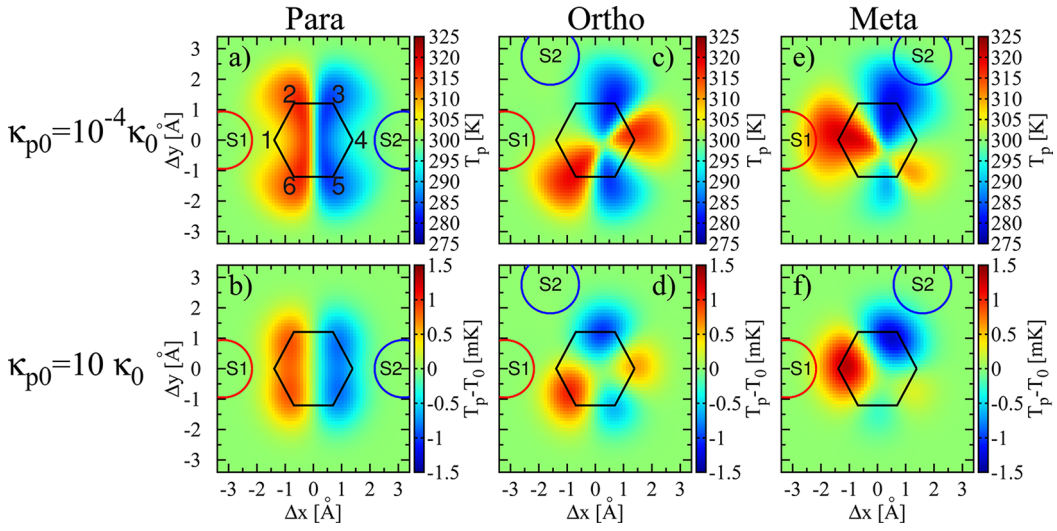

Figure 5. Calculated spatial temperature distributions of para ([1,4]BDT]), ortho ([1,2]BDT), and meta ([1,3]BDT) junctions measured by a Pt SThM scanned 3.5 Å above the plane of carbon nuclei with T_1 = 325 K and T_2 = 275 K. Each junction is shown for weak (upper panels) and strong (lower panels) SThM-environment coupling strengths. (a−d) Quantum oscillations of the temperature are clearly visible in the vicinity of the molecule, which can be explained in terms of the Kekulé contributing structures shown in Figure 7. (e, f) Temperature distribution of the meta junction exhibits well-defined "bond temperatures" arising from off-diagonal contributions to the thermal transport, in addition to the "orbital temperatures" of orbitals 1 and 3 proximal to the hot and cold electrodes, respectively. For these profiles, $\max\{S\} \approx 0.9$ for $\kappa_{p0} = 10^{-4}\kappa_0$ and $\max\{S\} \approx 1.1 \times 10^{-4}$ for $\kappa_{p0} = 10\kappa_0$, indicating temperature oscillations can be observed even with small sensitivities (see Methods section). The sulfur linker atoms are included in the transport calculations and are shown as red and blue circles, indicating the contacts to the hot and cold leads, respectively.

electrodes, respectively, have intermediate temperatures. Comparing the upper and lower panels of the same figure, we see that when the thermal coupling between the probe and the ambient environment is weaker, the thermal oscillations are observed over larger length scales, whereas stronger coupling reduces the resolution of these quantum effects. The calculated temperature distribution was found to be nearly independent of the strength of the tip−sample coupling Γ^p, except inasmuch as this affects the sensitivity S of the measurement (see Methods and Supporting Information).

Quantum oscillations of the temperature in a nanostructure subject to a temperature gradient are a thermal analogue of the voltage oscillations predicted by Büttiker[14] in a quantum system with an electrical bias. Similar temperature oscillations in one-dimensional quantum systems were first predicted by Dubi and Di Ventra.[11]

In order to understand the temperature oscillations shown in Figure 5, it is useful to consider the thermal conductance $\tilde{\kappa}_{p1}$ between the probe and the hot electrode. Figure 6a indicates that $\tilde{\kappa}_{p\beta}$ is large when the probe is in the ortho or para configuration relative to electrode β, as well as when it is proximal to the π-orbital directly coupled to the electrode. However, $\tilde{\kappa}_{p\beta}$ is nearly zero when the probe is in the meta configuration relative to electrode β. The three-terminal correction to the thermal conductance $\Delta\kappa_{p1}$ is plotted in Figure 6b, which indicates that three-terminal thermoelectric effects lead to a sizable relative correction to the thermal conductance between the probe and the electrode in the meta configuration, but are otherwise small.

When $\tilde{\kappa}_{p1} \gg \tilde{\kappa}_{p2}$, eq 8 implies the probe will measure a temperature near T_1, and *vice versa* when $\tilde{\kappa}_{p1} \ll \tilde{\kappa}_{p2}$, provided the coupling to the environment is not too large. On the other hand, the probe will measure a temperature near T_0 if $\tilde{\kappa}_{p1} \approx \tilde{\kappa}_{p2}$. Comparing the para temperature profile shown in Figure 5a,b to Figure 6, one sees that π-orbitals 2 and 6 are hot because when the SThM is coupled locally to them it is in an ortho configuration relative to the hot electrode and a meta configuration relative to the cold electrode, and $\tilde{\kappa}_{ortho} \gg \tilde{\kappa}_{meta}$. Orbitals 3 and 5 are cold by symmetry. On the other hand, orbitals 1 and 4 have intermediate temperatures since $\tilde{\kappa}_{p1} \approx \tilde{\kappa}_{p2}$ when the SThM is in a para configuration relative to one electrode and proximal to the other.

The quantum temperature oscillations in the para junction can also be understood in terms of the *rules of covalence* in conjugated systems. Figure 7 shows the Kekulé contributing structures illustrating charge transfer from an electrode E to a benzene molecule. Considering both hot and cold electrodes, the rules of covalence dictate that electrons from the hot electrode are available to tunnel onto the temperature probe when it is coupled locally to orbital 2, 4, or 6, while electrons from the cold electrode are available to tunnel when the probe is near orbital 1, 3, or 5. In addition, electrons from the hot electrode are available to tunnel onto the temperature probe when it is near

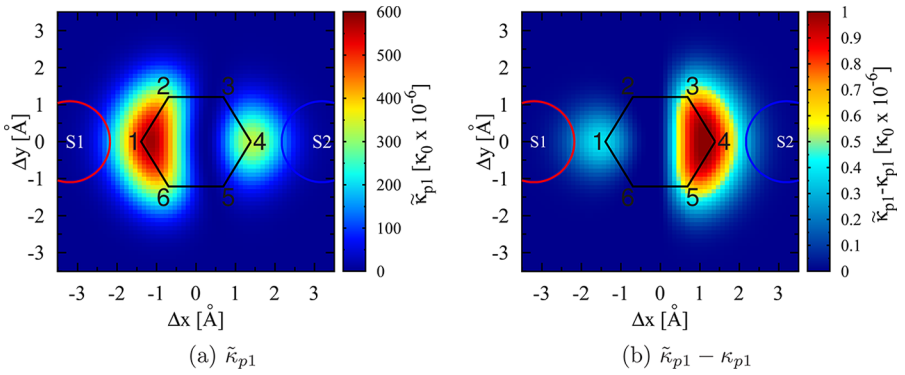

Figure 6. (a) Thermal conductance $\tilde{\kappa}_{p1}$ between lead 1 (hot) and the temperature probe *p*. $\tilde{\kappa}_{p1}$ is largest when *p* is in an ortho or para configuration relative to the hot electrode or proximal to it (near orbitals 1, 2, 4, or 6) and smallest when it is in a meta configuration relative to the hot electrode (near orbitals 3 and 5). (b) The difference between the three- and two-terminal thermal conductances, $\tilde{\kappa}_{p1} - \kappa_{p1}$, showing the largest errors ($1.03 \times 10^{-6}\kappa_0$) occurs where $\tilde{\kappa}_{p1}$ is small (near sites 3 and 5), indicating large relative errors if a two-terminal formulation were used. Here $\kappa_0 = (\pi^2/3)k_B^2T_0/h = 2.84 \times 10^{-10}$W/K with $T_0 = 300$ K.

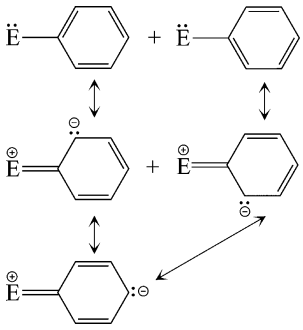

Figure 7. Kekulé contributing structures illustrating charge transfer from an electrode E onto benzene. Here a second line between atoms represents a double bond, a dot represents an unpaired electron, and (+) and (−) are the charges of the atoms in a given electronic configuration. Within resonance theory, the quantum state of the interacting system is given by a linear combination of these contributing structures. The rules of covalence in conjugated systems dictate that electrons from an electrode are available to tunnel onto the temperature probe when it is coupled locally to the molecule in an ortho or para configuration relative to the electrode.

orbital 1, which is proximal to the hot electrode, while electrons from the cold electrode are available to tunnel onto the temperature probe when it is near orbital 4, which is proximal to the cold electrode. Orbitals 2 and 6 thus appear hot, orbitals 3 and 5 appear cold, while orbitals 1 and 4 should exhibit intermediate temperatures by this argument.

The calculated temperature distribution of an ortho BDT junction is shown in Figure 5c,d, measured under the same conditions as the para junctions. The Kekulé contributing structures illustrated in Figure 7 dictate that lone pairs from the hot electrode may tunnel to orbital 2, 4, or 6, and lone pairs from the cold electrode may tunnel to orbital 1, 3, or 5. Taking into account that orbitals 1 and 2 are also proximal to the linker groups binding the molecule to the hot and cold electrodes, respectively, and thus exhibit intermediate temperatures, the rules of covalence dictate that orbitals 4 and 6 appear hot, while orbitals 3 and 5 appear cold, in complete agreement with the calculated temperature distribution.

For the para and ortho junctions the rules of covalence act essentially like a Maxwell demon, in that they selectively permit electrons from the hot or cold reservoir to tunnel onto the probe when it is at specific locations near the molecule and block electrons from the other reservoir. The situation is analogous to the "temperature demon",[37] wherein a tiny being controls the transfer of gas molecules between two containers, allowing only fast-moving molecules to flow from container 1 to container 2 and only slow-moving molecules to flow in the opposite sense, leading to a violation of the second law of thermodynamics. Rather than gas molecules, the present case involves electrons, while the molecular junction and metal tip of the SThM represent containers 1 and 2, respectively. When the temperature probe is at one of the hot spots in Figure 5, the rules of covalence do not allow electrons within the molecule, chosen at random, to tunnel onto the tip, but only electrons with an energy distribution characteristic of the hot reservoir—a distribution *hotter than the mean temperature of the molecule*. As the probe equilibrates at such a hot spot, heat is thus transferred from the molecule to the probe, whose temperature is higher than the mean temperature of the molecule.

The question might arise whether the actions of this would-be Maxwell demon could lead to a violation of the second law of thermodynamics, as Maxwell originally hypothesized. However, in this case there is no violation of the second law, because electrons within the molecule "remember" which electrode they came from. There is no "mixing" of the hot and cold electrons in the absence of inelastic scattering, which is strongly suppressed compared to elastic processes in these junctions at room temperature.

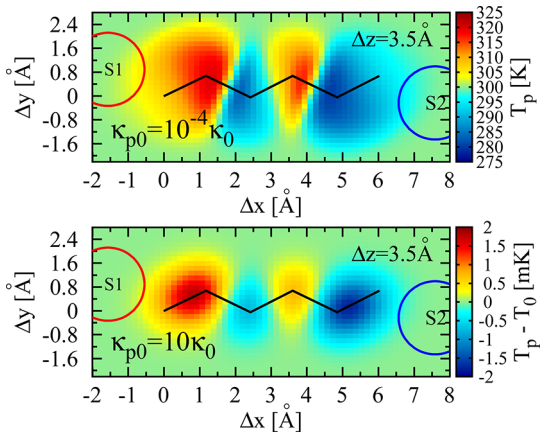

Figure 8. Calculated temperature distribution for a Au–[1,6]hexatrienedithiol–Au molecular junction, measured under the same conditions discussed in Figure 5. The observed temperature oscillations can be explained using the resonance contributing structures shown in Figure 9.

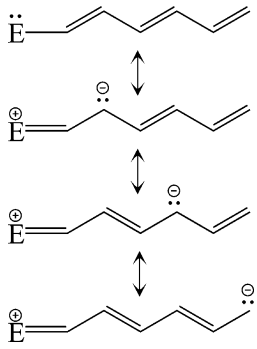

Figure 9. Resonance contributing structures for a hexatriene junction. For a given electrode E, the lone pair can occupy only every other π-orbital, giving rise to the alternating hot, cold temperature profile shown in Figure 8.

The calculated temperature distribution of a meta BDT junction is shown in the rightmost panels of Figure 5. In this case, the temperature distribution is more complicated, exhibiting both well-defined "orbital temperatures" (1 and 3) and "bond temperatures" (4–5 and 5–6 bonds). The temperatures of orbitals 1 and 3 can be explained by the arguments given above, while the rules of covalence illustrated in Figure 7 indicate that *electrons from neither the hot electrode nor the cold electrode can reach orbital 5*, so that its temperature is indeterminate. Near orbital 5, off-diagonal contributions to the transmission dominate due to the suppression of transmission in the meta configuration. The para transmission amplitude interferes constructively with the small but nonzero meta transmission amplitude, while the ortho transmission amplitude interferes destructively with the meta transmission amplitude, so that the 4–5 bond appears hot, while the 5–6 bond appears cold.

[1,6]Hexatrienedithiol Junction. The calculated temperature distribution of a [1,6]hexatrienedithiol junction composed of a thioloated six-site linear molecule (hexatriene) covalently bonded to two gold electrodes is shown in Figure 8. The conditions of the temperature measurement are the same as described in Figure 5. Quasi-one-dimensional temperature oscillations are clearly observable along the length of the molecular wire, consistent with the prediction of ref 11. The resonance contributing structures describing electron transfer from an electrode E onto the molecule are shown in Figure 9. As in the case of the para and ortho BDT junctions, the rules of covalence are unambiguous and predict alternating hot and cold temperatures for the π-orbitals along the length of the molecule, with intermediate temperatures for the end orbitals proximal to the two electrodes, consistent with the calculated temperature distribution.

[2,7]Pyrenedithiol Junction. As a final example, we consider the effects of finite spatial resolution on the measured temperature distribution of a polycyclic [2,7]pyrenedithiol–Au junction. The temperature distribution was calculated for three different values of the SThM spatial resolution in the three panels of Figure 10: The leftmost panel shows the maximum spatial resolution under the specifications of a hypothetical SThM described in Figure 5. The middle and rightmost panels show the measured temperature distributions with reduced spatial resolution obtained by convolving the tip–sample tunnel-coupling Γ^p with Gaussian distributions with standard deviations of σ = 0.5 and 1.0 Å, respectively (full resolution corresponds to σ = 0). Many-body transport calculations for this larger molecule are currently computationally intractable, so we have utilized Hückel theory to describe the molecular electronic structure (see Supporting Information).

The leftmost panel of Figure 10 shows a complex interference pattern of hot and cold regions with a symmetry that mimics the junction itself (in this case with two mirror axes). More complex molecules such as this highlight the "proximity effect" whereby the flow of heat from a given electrode to the orbitals in its vicinity is enhanced, so the molecule is generally warmer near the hot lead and cooler near the cold lead. We mention that, although more tedious, the Kekulé contributing structures[38] can be used to understand the pattern of temperature variations in this molecule as well.

Focusing on the middle and rightmost panels of Figure 10, we find an immediate consequence of the proximity effect as σ is increased: nonmonotonic temperature variations due to quantum interference are washed out, and the underlying temperature gradient appears. In the rightmost panel, quantum temperature oscillations are no longer resolved, and the temperature distribution resembles a thermal dipole. Similar results were obtained for a variety of molecular junctions, suggesting that a classical temperature distribution consistent with Fourier's law of heat

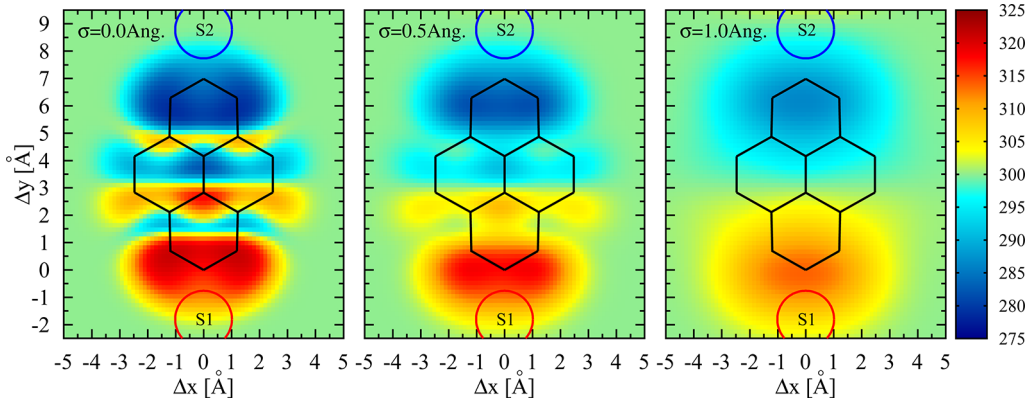

Figure 10. Calculated spatial temperature distribution for a Au−[2,7]pyrenedithiol−Au junction with T_1 = 325 K and T_2 = 275 K, measured at a height of 3.5 Å above the plane of the molecule, for three different values of SThM spatial resolution. The leftmost panel shows the maximum spatial resolution under the specifications of a hypothetical SThM described in Figure 5. The middle and rightmost panels show the measured temperature distributions with reduced spatial resolution obtained by convolving the tip−sample tunnel-coupling Γ^p with Gaussian distributions with standard deviations of σ = 0.5 and 1.0 Å, respectively (full resolution corresponds to σ = 0). In the rightmost panel, quantum temperature oscillations are no longer resolved, and the temperature distribution resembles a thermal dipole. Similar results were obtained for a variety of molecular junctions, suggesting that a classical temperature distribution consistent with Fourier's law of heat conduction emerges due to measurements with limited spatial resolution.

conduction emerges when the temperature is measured with limited spatial resolution.

The transition from microscopic quantum temperature oscillations to macroscopic diffusive behavior and Fourier's law is still poorly understood.[24] It has been argued that Fourier's law is recovered in systems with sufficient dephasing[6] or disorder.[7] However, we have seen that in conjugated organic molecules the quantum temperature oscillations are intimately connected to the rules of covalence describing the π-bonds of the molecule. Dephasing (or disorder) sufficient to wash out the temperature oscillations would thus necessarily sever the π-bonds and dissociate the molecule. Since the molecules studied in this article are stable at room temperature, we know that such strong dephasing cannot be present. Thus we predict that quantum temperature oscillations will be observed in molecular junctions if temperature measurements with sufficient spatial resolution are performed and that Fourier's law is a consequence of coarse-graining due to finite spatial resolution.

CONCLUSIONS

We have proposed a physically motivated and mathematically rigorous definition of an electron thermometer as an electron reservoir coupled locally to and in both thermal and electrical equilibrium with the system being measured [*cf.* eq 1]. This definition is valid under general nonequilibrium conditions with arbitrary thermal and/or electric bias. On the basis of this definition, we have developed a realistic model of an atomic-resolution SThM operating in the tunneling regime in ultrahigh vacuum, including the effect of thermal coupling of the probe to the ambient environment.

We used this model of an atomic-resolution SThM to investigate the nonequilibrium temperature distributions of a variety of single-molecule junctions subject to thermal gradients. Quantum oscillations of the local temperature that can be observed using an SThM with sufficiently high resolution are predicted. We show that in many cases these quantum temperature oscillations may be understood straightforwardly in terms of the rules of covalence describing bonding in π-electron systems. As such, these oscillations are predicted to be extremely robust, insensitive to dephasing or disorder that is insufficient to dissociate the molecule. Instead, we show that such quantum interference effects are washed out if the spatial resolution of the SThM is insufficient to observe them and that the temperature distribution then approaches that expected based on Fourier's classical law of heat conduction. Reduced thermal resolution of the SThM *does not* wash out the temperature oscillations, but merely reduces their observed amplitude.

One may wonder whether it is meaningful to define a temperature that varies significantly from place to place at the atomic scale. Since temperature is related to mean thermal energy, does a variation of temperature on a scale comparable to the de Broglie wavelength not violate the uncertainty principle? Our answer to such questions is a pragmatic one: By definition, temperature is that which is measured by a thermometer, and the position of a thermometer can certainly be controlled with subatomic precision using standard scanning probe techniques. We should also emphasize that our proposed thermometer measures the *electron temperature*, which may be largely decoupled from the *lattice temperature* in nanoscale junctions.

Finally, let us return to the theme of the title of this article. We have shown that in a molecular junction containing a conjugated organic molecule, the rules of covalence act essentially like a Maxwell demon, in that they selectively permit electrons from the hot or cold

reservoir to tunnel onto the probe, when it is at specific locations near the molecule, and block electrons from the other reservoir. The question might arise whether the actions of this Maxwell demon could lead to a violation of the second law of thermodynamics, as Maxwell originally hypothesized. However, in this case there is no violation of the second law, because electrons within the molecule "remember" which electrode they came from. There is no "mixing" of the hot and cold electrons in the absence of inelastic scattering, and we have argued that dephasing due to inelastic scattering is insufficient to perturb this particular embodiment of Maxwell's demon without dissociating the molecule itself.

METHODS

Molecular Dyson Equation Many-Body Quantum Transport Theory. In the energy domain and using matrix notation, the Green's function of a molecular junction may be expressed exactly *via* the molecular Dyson equation (MDE) as[13]

$$G = G_{mol} + G_{mol}\Sigma G \tag{17}$$

where G_{mol} is the interacting molecular Green's function found in the limit of weak tunnel coupling to the electrodes, but including long-range Coulomb interactions between the π-electrons. The self-energy $\Sigma = \Sigma_T + \Delta\Sigma_C$, where Σ_T is the tunneling self-energy associated with the lead-molecule bonds and $\Delta\Sigma_C$ is the correction to the Coulomb self-energy arising from lead-molecule coherence. The molecular Dyson equation is exact: the derivation of eq 17 requires no approximations.[13] MDE theory describes both Coulomb blockade (particle-like) and resonant tunneling (wave-like) effects simultaneously, both of which are important in molecular junction transport experiments. Away from resonance and at room temperature $\Delta\Sigma_C \approx 0$, an approximation that is discussed in detail in ref 13.

The tunneling self-energy associated with a given electrode can be expressed as $\Sigma_T^\alpha = V^\alpha g^\alpha(E)[V^\alpha]^\dagger$, where $g^\alpha(E)$ is the retarded Green's function for lead α, and V^α describes the tunneling between lead α and the molecule. In the wide-band limit the energy dispersion of the electrode is assumed to be slowly varying and the tunneling self-energy is given by

$$\Sigma_T = -\frac{i}{2}\sum_\alpha \Gamma^\alpha \tag{18}$$

where Γ^α is the tunneling-width matrix associated with lead α.

Aside from the self-energy, the other ingredient needed to evaluate eq 17 is the Green's function of the isolated molecule. This is determined exactly (in the limited Hilbert space of the π-electrons) by first finding the few-body eigenstates $|\nu\rangle$ and eigenenergies E_ν of the isolated molecule and then using these to explicitly evaluate the molecular Green's function:[13]

$$G_{mol} = \sum_{\nu,\nu'} \frac{[P(\nu) + P(\nu')]C(\nu,\nu')}{E - (E_{\nu'} - E_\nu) + i0^+} \tag{19}$$

Here $P(\nu)$ is the statistical occupancy of the νth eigenstate, given at equilibrium by the grand canonical ensemble (sufficient for linear response transport calculations), and

$$C_{n\sigma,m\sigma'}(\nu,\nu') = \langle\nu|d_{n\sigma}|\nu'\rangle\langle\nu'|d^\dagger_{m\sigma'}|\nu\rangle \tag{20}$$

are many-body matrix elements. $d^\dagger_{m\sigma}$ creates an electron with spin σ in the mth π-orbital of the molecule.

Equations 17−20 provide a method for obtaining the full interacting Green's function of the molecule coupled to the electrodes, which may then be used to calculate the various physical quantities of interest. For instance, the heat and charge currents given by eq 2 involve $G(E)$ *via* eqs 12 and 13.

Equilibration Time for a Nanoscale Thermometer. The heat capacity of the probe must be sufficiently small to ensure an equilibration time that is less than any drift times in an experimental system. Using eq 3, we have

$$I_p^{(1)} \equiv CV\frac{dT_p}{dt} = \tilde{\kappa}_{p1}(T_1 - T_p) + \tilde{\kappa}_{p2}(T_2 - T_p) + \kappa_{p0}(T_0 - T_p) \tag{21}$$

where $I_p^{(1)}$ is the heat current into the probe, and C and V are the heat capacity and volume of the metal tip of the probe, respectively. Equation 21 leads to the following first-order differential equation:

$$\frac{dT_p}{dt} = \tau^{-1}(\bar{T}_p - T_p) \tag{22}$$

where

$$\bar{T}_p = \frac{\tilde{\kappa}_{p1}T_1 + \tilde{\kappa}_{p2}T_2 + \kappa_{p0}T_0}{\tilde{\kappa}_{p1} + \tilde{\kappa}_{p2} + \kappa_{p0}} \tag{23}$$

and the equilibration time of the temperature probe is given by

$$\tau = \frac{CV}{\tilde{\kappa}_{p1} + \tilde{\kappa}_{p2} + \kappa_{p0}} \tag{24}$$

For a Pt probe tip with linear dimensions on the order of 1 μm, $V \le 4/3\pi r^3 = 4.19 \times 10^{-12}$ cm^3, and $CV \le 1.17 \times 10^{-11}$ J/K, where the specific heat C_{Pt} = (133 J/kgK) × (0.021 kg/cm^3).[32] The spatial equilibration time profiles for such a Pt probe fixed 3.5 Å

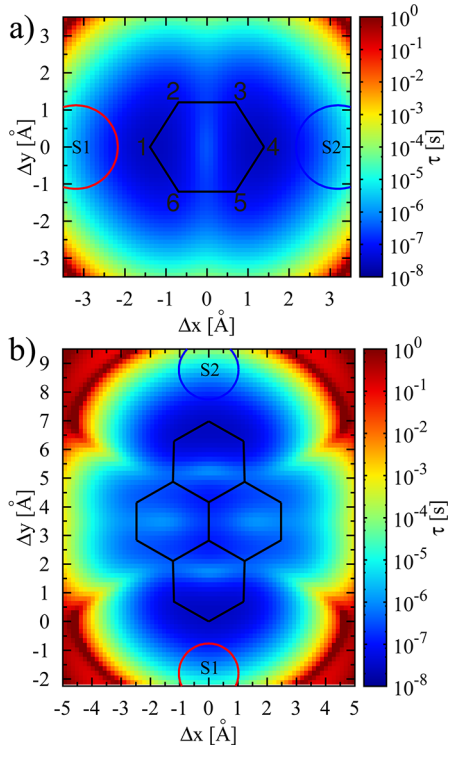

Figure 11. Calculated equilibration time of a Pt SThM probe fixed 3.5 Å above (a) a Au−[1,4]BDT−Au junction and (b) a Au−[2,7]pyrenedithiol−Au junction. These equilibration times are *upper bounds* since we set $\kappa_{p0} = 0$. The SThM tip's volume was taken to be that of a sphere with a diameter of 1 μm.

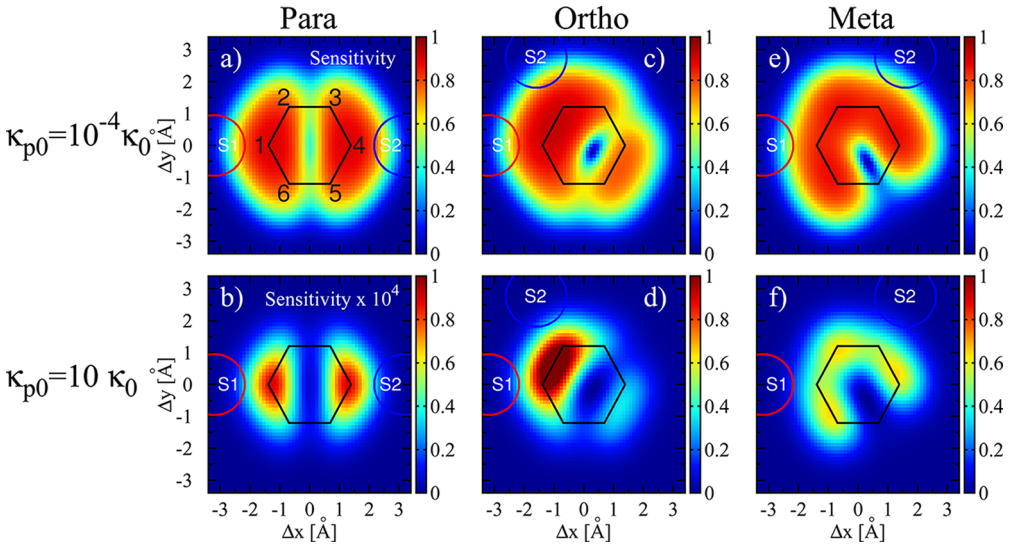

Figure 12. Calculated sensitivity distributions for para-, ortho-, and meta-configured BDT junctions measured using a Pt SThM probe scanned 3.5 Å above the plane of the molecules. The temperature profile of each junctions is shown in Figure 5. All data here were simulated under the same conditions. In spite of the low sensitivity when $\kappa_{p0} = 10\kappa_0$, quantum oscillations in the temperature profile are still clearly visible in Figure 5.

above a Au−[1,4]BDT−Au and a Au−[2,7]pyrenedithiol−Au junction are shown in panels a and b of Figure 11, respectively. All calculations are performed with $\kappa_{p0} = 0$ and are thus upper bounds on the true equilibration time given by eq 24. In both cases, the equilibration times are on the order of tens of nanoseconds when the SThM is above the molecule.

Sensitivity. The sensitivity profiles of para-, ortho-, and meta-configured BDT junctions measured using a Pt SThM probe scanned 3.5 Å above the plane of the molecule are shown in Figure 12. These simulations indicate that even with low sensitivity (*i.e.*, when $\kappa_{p0} = 10\kappa_0$) the quantum oscillations of the temperature (*cf.* Figure 5) are still experimentally resolvable. With current experimental techniques $\kappa_{p0} \approx 700\kappa_0$, which gives a temperature range of $\sim$30 μK for the BDT junctions discussed here. In order to experimentally observe these quantum temperature oscillations, the environmental coupling to the probe will have to be decreased and/or the temperature precision increased.

Conflict of Interest: The authors declare no competing financial interest.

Acknowledgment. This material is based on work supported by the Department of Energy under Award No. DE-SC0006699.

Supporting Information Available: Additional simulations and analyses include here: the effect of different lead-molecule coupling and asymmetric temperature bias on the predicted quantum temperature oscillations, an electrostatic model to include the thiol linker groups and electrodes, and the details of the electronic model used in the pyrene transport calculations. This material is available free of charge *via* the Internet at http://pubs.acs.org.

REFERENCES AND NOTES

1. Majumdar, A. Scanning Thermal Microscopy. *Annu. Rev. Mater. Sci.* **1999**, *29*, 505–585.
2. Kim, K.; Chung, J.; Hwang, G.; Kwon, O.; Lee, J. S. Quantitative Measurement with Scanning Thermal Microscope by Preventing the Distortion Due to the Heat Transfer through the Air. *ACS Nano* **2011**, *5*, 8700–8709.
3. Yu, Y.-J.; Han, M. Y.; Berciaud, S.; Georgescu, A. B.; Heinz, T. F.; Brus, L. E.; Kim, K. S.; Kim, P. High-Resolution Spatial Mapping of the Temperature Distribution of a Joule Self-Heated Graphene Nanoribbon. *Appl. Phys. Lett.* **2011**, *99*, 183105.
4. Kim, K.; Jeong, W.; Lee, W.; Reddy, P. Ultra-High Vacuum Scanning Thermal Microscopy for Nanometer Resolution Quantitative Thermometry. *ACS Nano* **2012**, *6*, 4248–4257.
5. Menges, F.; Riel, H.; Stemmer, A.; Gotsmann, B. Quantitative Thermometry of Nanoscale Hot Spots. *Nano Lett.* **2012**, *12*, 596–601.
6. Dubi, Y.; Di Ventra, M. Fourier's Law: Insight from a Simple Derivation. *Phys. Rev. E* **2009**, *79*, 042101.
7. Dubi, Y.; Di Ventra, M. Reconstructing Fourier's Law from Disorder in Quantum Wires. *Phys. Rev. B* **2009**, *79*, 115415.
8. Engquist, H.-L.; Anderson, P. W. Definition and Measurement of the Electrical and Thermal Resistances. *Phys. Rev. B* **1981**, *24*, 1151–1154.
9. Caso, A.; Arrachea, L.; Lozano, G. S. Local and Effective Temperatures of Quantum Driven Systems. *Phys. Rev. B* **2010**, *81*, 041301.
10. Ming, Y.; Wang, Z. X.; Ding, Z. J.; Li, H. M. Ballistic Thermal Rectification in Asymmetric Three-Terminal Mesoscopic Dielectric Systems. *New J. Phys* **2010**, *12*, 103041.
11. Dubi, Y.; Di Ventra, M. Thermoelectric Effects in Nanoscale Junctions. *Nano Lett.* **2009**, *9*, 97–101.
12. Galperin, M.; Nitzan, A.; Ratner, M. A. Heat Conduction in Molecular Transport Junctions. *Phys. Rev. B* **2007**, *75*, 155312.
13. Bergfield, J. P.; Stafford, C. A. Many-Body Theory of Electronic Transport in Single-Molecule Heterojunctions. *Phys. Rev. B* **2009**, *79*, 245125.
14. Büttiker, M. Chemical Potential Oscillations Near a Barrier in the Presence of Transport. *Phys. Rev. B* **1989**, *40*, 3409–3412.
15. Reddy, P.; Jang, S.-Y.; Segalman, R. A.; Majumdar, A. Thermoelectricity in Molecular Junctions. *Science* **2007**, *315*, 1568–1571.
16. Baheti, K.; Malen, J.; Doak, P.; Reddy, P.; Jang, S.-Y.; Tilley, T.; Majumdar, A.; Segalman, R. Probing the Chemistry of Molecular Heterojunctions Using Thermoelectricity. *Nano Lett.* **2008**, *8*, 715–719.
17. Bergfield, J. P.; Solis, M. A.; Stafford, C. A. Giant Thermoelectric Effect from Transmission Supernodes. *ACS Nano* **2010**, *4*, 5314–5320.
18. Yee, S. K.; Malen, J. A.; Majumdar, A.; Segalman, R. A. Thermoelectricity in Fullerene-Metal Heterojunctions. *Nano Lett.* **2011**, *11*, 4089–4094.
19. Caso, A.; Arrachea, L.; Lozano, G. S. Relation Between Local Temperature Gradients and the Direction of Heat Flow in Quantum Driven Systems. *Phys. B (Amsterdam, Neth.)* **2012**, *407*, 3172–3174.
20. Sánchez, D.; Serra, L. Thermoelectric Transport of Mesoscopic Conductors Coupled to Voltage and Thermal Probes. *Phys. Rev. B* **2011**, *84*, 201307.

21. Jacquet, P. A.; Pillet, C.-A. Temperature and Voltage Probes Far from Equilibrium. *Phys. Rev. B* **2012**, *85*, 125120.
22. Caso, A.; Arrachea, L.; Lozano, G. S. Local Temperatures and Heat Flow in Quantum Driven Systems. *Phys. Rev. B* **2011**, *83*, 165419.
23. Caso, A.; Arrachea, L.; Lozano, G. S. Defining the Effective Temperature of a Quantum Driven System from Current-Current Correlation Functions. *Eur. Phys. J. B* **2012**, *85*, 266.
24. Dubi, Y.; Di Ventra, M. *Colloquium*: Heat Flow and Thermoelectricity in Atomic and Molecular Junctions. *Rev. Mod. Phys.* **2011**, *83*, 131–155.
25. Ziman, J. M. *Principles of the Theory of Solids*, 2nd ed.; Cambridge University Press: London, 1972.
26. Sivan, U.; Imry, Y. Multichannel Landauer Formula for Thermoelectric Transport with Application to Thermopower Near the Mobility Edge. *Phys. Rev. B* **1986**, *33*, 551–558.
27. Bergfield, J. P.; Stafford, C. A. Thermoelectric Signatures of Coherent Transport in Single-Molecule Heterojunctions. *Nano Lett.* **2009**, *9*, 3072–3076.
28. Datta, S. *Electronic Transport in Mesoscopic Systems*; Cambridge University Press: Cambridge, UK, 1995.
29. Chen, C. J. *Introduction to Scanning Tunneling Microscopy*, 2nd ed.; Oxford University Press: New York, 1993.
30. Bergfield, J. P.; Barr, J. D.; Stafford, C. A. Transmission Eigenvalue Distributions in Highly Conductive Molecular Junctions. *Beilstein J. Nanotechnol.* **2012**, *3*, 40–51.
31. Xiao, X.; Xu, B.; Tao, N. Measurement of Single Molecule Conductance: Benzenedithiol and Benzenedimethanethiol. *Nano Lett.* **2004**, *4*, 267–271.
32. Lide, D. R., Ed. *CRC Handbook of Chemistry and Physics*; CRC Press: Boca Raton, FL, 2005.
33. Rego, L. G. C.; Kirczenow, G. Quantized Thermal Conductance of Dielectric Quantum Wires. *Phys. Rev. Lett.* **1998**, *81*, 232–235.
34. Rego, L. G. C.; Kirczenow, G. Fractional Exclusion Statistics and the Universal Quantum of Thermal Conductance: A Unifying Approach. *Phys. Rev. B* **1999**, *59*, 13080–13086.
35. Rocheleau, T.; Ndukum, T.; Macklin, C.; Hertzberg, J. B.; Clerk, A. A.; Schwab, K. C. Preparation and Detection of a Mechanical Resonator Near the Ground State of Motion. *Nature* **2010**, *463*, 72–75.
36. Biehs, S.-A.; Rousseau, E.; Greffet, J.-J. Mesoscopic Description of Radiative Heat Transfer at the Nanoscale. *Phys. Rev. Lett.* **2010**, *105*, 234301.
37. Maruyama, K.; Nori, F.; Vedral, V. *Colloquium*: The Physics of Maxwell's Demon and Information. *Rev. Mod. Phys.* **2009**, *81*, 1–23.
38. Camerman, A.; Trotter, J. The Crystal and Molecular Structure of Pyrene. *Acta Crystallogr.* **1965**, *18*, 636–643.